CHEMISTRY
A EUROPEAN JOURNAL

ChemPubSoc
Europe

DOI: 10.1002/chem.201102637

Photomagnetism of a *sym-cis*-Dithiocyanato Iron(II) Complex with a Tetradentate *N*,*N*′-Bis(2-pyridylmethyl)1,2-ethanediamine Ligand

Jean-François Létard,*[a] Saket Asthana,[a, d] Helena J. Shepherd,[c] Philippe Guionneau,[a] André E. Goeta,[c] Naohiko Suemura,[b] Ryuta Ishikawa,[b] and Sumio Kaizaki[b]

In memory of André E. Goeta

Abstract: A comprehensive study of the magnetic and photomagnetic behaviors of *cis*-[Fe(picen)$(NCS)_2$] (picen = *N*,*N*′-bis(2-pyridylmethyl)1,2-ethanediamine) was carried out. The spin-equilibration was extremely slow in the vicinity of the thermal spin-transition. When the cooling speed was slower than 0.1 K min^{-1}, this complex was characterized by an abrupt thermal spin-transition at about 70 K. Measurement of the kinetics in the range 60–70 K was performed to approach the quasi-static hysteresis loop. At low temperatures, the metastable HS state was quenched by a rapid freezing process and the critical *T*(TIESST) temperature, which was associated with the thermally induced excited spin-state-trapping (TIESST) effect, was measured. At 10 K, this complex also exhibited the well-known light-induced excited spin-state-trapping (LIESST) effect and the *T*(LIESST) temperature was determined. The kinetics of the metastable HS states, which were generated from the freezing effect and from the light-induced excitation, was studied. Single-crystal X-ray diffraction as a function of speed-cooling and light conditions at 30 K revealed the mechanism of the spin-crossover in this complex as well as some direct relationships between its structural properties and its spin state. This spin-crossover (SCO) material represents a fascinating example in which the metastability of the HS state is in close vicinity to the thermal spin-transition region. Moreover, it is a beautiful example of a complex in which the metastable HS states can be generated, and then compared, either by the freezing effect or by the LIESST effect.

Keywords: iron · ligand effects · photomagnetism · spin crossover · X-ray diffraction

Introduction

The development of materials that allow us to obtain information at the single-molecular level or on assemblies of molecules is important for the future development of information technology.[1] Among all of the reported systems, one interesting class of molecular switches are those that involve the light-induced excited spin-state-trapping (LIESST) phenomenon.[2–5] Materials of this kind combine: 1) low addressing power (about 5 mW cm^{-2}); 2) short addressing time (nanosecond scale); 3) perfect reproducibility over successive cycles, even in a solid matrix; and 4) optical reversibility. The low-spin (LS, $^1A_1$)→high-spin (HS, $^5T_2$) transition in iron(II) spin-crossover (SCO) materials can be induced with green light and the back-conversion to the LS state can be induced with red light. In fact, the main limitation comes from the stability of the photoinduced metastable HS state. Below 50 K, the lifetime is almost infinite and optical data storage can be envisaged, whilst at higher temperatures, the relaxation is governed by the activated regime and the photoinduced HS state decays within seconds or less. To overcome this limitation, it has been recently reported that, in some iron(II) molecular materials, the light-induced phenomenon can be generated in the center of a thermal hysteresis.[4] However, the integration of such molecular systems into a "real" device[5] would require an iron(II) spin-crossover (SCO) material with a thermal hysteresis loop of around 100 K in width, a value that has not yet been reached.

An alternative strategy is to identify the factors that influence the stability of the light-induced metastable state at low temperatures, that is, outside the thermal hysteresis, through the LIESST phenomenon.[3] Along these lines, we

[a] Dr. J.-F. Létard, Dr. S. Asthana, Dr. P. Guionneau
CNRS, Université Bordeaux, ICMCB
Groupe des Sciences Moléculaires
87 Av. Doc. A. Schweitzer, 33608 Pessac (France)
Fax: (+33) (0)540002678
E-mail: letard@icmcb-bordeaux.cnrs.fr

[b] N. Suemura, R. Ishikawa, Prof. S. Kaizaki
Department of Chemsitry, Graduate School of Science
Osaka University, Toyonaka
Osaka, 540-0043 (Japan)

[c] H. J. Shepherd, Dr. A. E. Goeta
Crystallography group, Durham University
Durham DH1 3LE (UK)

[d] Dr. S. Asthana
Present address:
Department of Physics, Indian Institute of Technology
Hyderabad (India)

introduced the idea of systematically determining the *T*-(LIESST) value,[6a] which represents the limiting temperature above which the light-induced magnetic HS information is erased when the temperature in a SQUID magnetometer is increased at a rate of 0.3 K min^{-1}. Using this procedure, we compared the photomagnetic properties of more than sixty SCO materials[6,7] and we found that factors such as cooperativity, the nature of the salt, and the degree of hydration had a relatively negligible effect on the stability of the metastable state.[8,9] In contrast, the influence of the inner FeN_6 coordination sphere, owing to the nature of the ligand, appeared to have a significant effect on the stabilization of the photoinduced HS state.[9,10] Following this idea, we focused our attention on macrocyclic ligands[11] and we recently demonstrated that an $[Fe(L_{222}N_5)(CN)_2]\cdot H_2O$ iron(II) complex with the $L_{222}N_5$ macrocyclic Schiff-base ligand 2,13-dimethyl-3,6,9,12,18-pentaazabicyclo[12.3.1]octadeca-1(18),2,12,14,16-pentaene, which was low-spin at up to about 400 K, exhibited an exceptionally long-lived photoinduced HS state, with a *T*(LIESST) temperature of about 105 K.[11a] In other words, modifying the inner coordination sphere appeared to be a promising strategy for stabilizing the metastable HS state. Such an alteration around the iron(II) metal center seemed to affect the kinetics of the structural rearrangement that accompanied the photoinduced HS→LS relaxation by acting on the vibrational properties[3g,12] and/or by distorting the inner core of the complex.

We investigated the photomagnetic properties of *cis*-[Fe(picen)$(NCS)_2$], which employed a tetradentate ligand, picen = *N*,*N*′-bis(2-pyridylmethyl)1,2-ethanediamine (Scheme 1) that was originally synthesized by Toftlund et al.[13] These authors, and later Gütlich and co-workers[14] and Kaizaki and co-workers[15], reported that this complex exhibited a more or less incomplete thermal spin-transition at around 70 K with the possibility of trapping the HS state at low temperatures by rapid freezing. Herein, we report a detailed study of the photomagnetic properties and a Raman characterization of this complex. The potential of this complex for exhibiting metastable HS states that were either generated by freezing (named HS_2) or by light irradiation (named HS_3) is discussed.

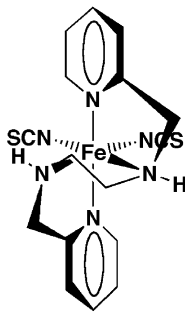

Scheme 1. The *cis*-diisothiocyanato-*N*,*N*′-bis(2-pyridylmethyl)1,2-ethanediamine iron(II) complex.

Results and Discussion

Magnetic studies: Figure 1 shows the magnetic data of the complex as function of the cooling rate. The magnetic response is expressed as $\chi_M T$ versus *T*, where χ_M is the molar magnetic susceptibility and *T* is the temperature. At room temperature, the $\chi_M T$ value (about 3.3 cm^3 K mol^{-1}) was within the expected region for a HS iron(II) center. When the temperature was lowered, in agreement with the report by Toflund et al.,[13] the importance of the HS fraction depended on the cooling rate. When the sample was cooled at a rate of 7 K min^{-1}, the $\chi_M T$ product gradually decreased and no thermal spin-transition was clearly observed. The residual HS faction (γ_{HS}), which was deduced from the ratio $\chi_M T/(\chi_M T)_{HT}$, where $(\chi_M T)_{HT}$ represented the magnetic response of the HS state at high temperature, was almost equal to 0.68 at 40 K, where the influence of the zero-field splitting was negligible. During a subsequent raising of the temperature, the magnetic signal exhibited an unusual decrease at about 67 K, and then increased at about 70 K to recover the magnitude of the HS state. When the cooling rate was 0.5 K min^{-1}, the thermal spin-transition became clearer. The HS faction at 40 K was 0.36 and the unusual bump during warming became less-pronounced. In fact, it was only when the cooling rate was slower than 0.1 K min^{-1} that the thermal spin-transition was almost complete. The residual HS fraction at 40 K was 0.09. On warming, a classical spin-transition occurred with an unusual bump at around 65 K. $T_{1/2}(\downarrow)$ and $T_{1/2}(\uparrow)$, which define the temperatures at which there is 50 % of both LS and HS molecules during the cooling and warming modes, respectively, were 65 K and 71 K, which led to a hysteresis loop of about 6 K. These data demonstrated that the spin-equilibration in this compound was very slow, particularly in the vicinity of the thermal spin-transition. As a consequence, even if the cooling speed was very slow, that is, 0.1 K min^{-1}, the measured hysteresis would remain an apparent one, as demonstrated by the unsymmetrical form of the cooling branch versus the warming branch. In fact, the "real" hysteresis loop would only be obtained by recording the hysteresis loop over an infinite time, that is, when a steady state between the population and relaxation is achieved. Otherwise, we are dealing with a dynamic hysteresis.

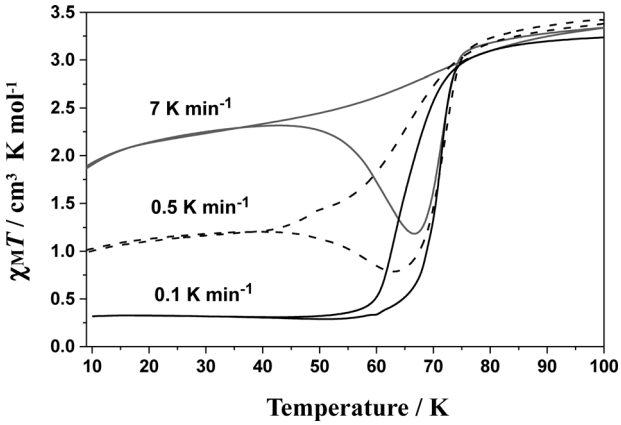

Figure 1. Magnetic properties as a function of the temperature and cooling rate for both the cooling and warming modes.

To approach the final form of the quasi-static (that is, real) hysteresis loop, we determined some stationary points on the cooling branch. We used the following procedure:

The sample was rapidly frozen from 290 K to a given temperature (T_Q) over a few seconds and the $\chi_M T$ product was recorded as a function of time. The experiment was stopped when the stationary limit, that is, spin-equilibration, was reached, typically after 5 h. The temperature was finally raised to 290 K and maintained at this temperature for 5 min to ensure that any LS fraction was erased. Sequentially, the T_Q value was fixed at 60, 62, 65, 67, and 70 K. Figure 2 shows the different kinetics and stationary limits, as well as a proposed profile of the "real" hysteresis curve. As expected, this hysteresis was much narrower than the "apparent" one, that is, about 2 K, as compared to 6 K (see above). Interestingly, the character of the real hysteresis loop was almost symmetric.

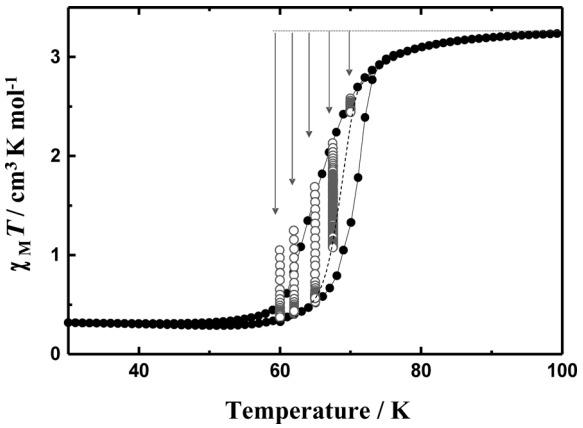

Figure 2. Evolution of the $\chi_M T$ product versus T (●) at a cooling rate of 0.1 K min^{-1} and a warming rate of 0.3 K min^{-1}. These parameters give the apparent hysteresis loop. (○) Kinetics of the quenched HS state for different temperatures; each relaxation leads to a stationary limit that describes the quasi-static hysteresis loop (– – –).

Quenched metastable HS state, HS_2: In their original work, Toflund et al.[13] reported that the metastable HS phase could be trapped by rapid freezing. Along those lines, Figure 3 shows the magnetic response after freezing. Rapid-freezing experiments were performed by cooling the cane from room temperature to 10 K over a few seconds. The magnetic response was then recorded and the temperature was slowly warmed at a rate of 0.3 K min^{-1}, which corresponded to the measurements on a T(TIESST) curve. These data revealed a decrease in the magnetic signal in the range 10–20 K, owing to the zero-field splitting (and thermal population of the higher levels) of a HS iron(II) metal center in pseudo-octahedral surroundings.[16] At around 20–30 K, the magnetic signal was more or less constant at 3.19 cm^3 mol^{-1} K, which was close to that of the HS phase (3.28 cm^3 mol^{-1} K at 110 K). This result indicated that the metastable HS_2 phase was quantitatively trapped at low temperatures and, moreover, that the relaxation process was extremely slow up to 30 K with regards to the time needed for recording the T(TIESST) curve. Consequently, the relaxation process was clearly governed by the tunneling regime

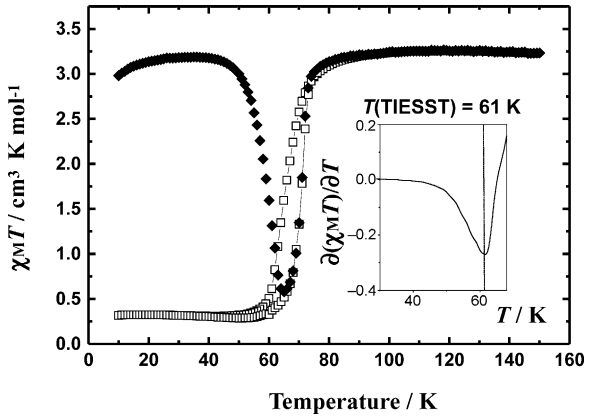

Figure 3. Temperature-dependence of the $\chi_M T$ value of the metastable HS state that was generated at 10 K by rapid freezing. (◆) Data recorded in the warming mode (0.3 K min^{-1}) after the trapping effect; (□) Data recorded in the cooling (0.1 K min^{-1}) and warming modes (0.3 K min^{-1}). Insets show the derivate of the $d\chi_M T/dT$ curves, whose minimum corresponds to the T(TIESST) temperature.

over this temperature range.[17] Such a situation was in contrast to the behavior at higher temperatures, where at around 45 K, the $\chi_M T$ product started to decrease dramatically, before finally returning to its initial value at 65 K and following the warming curve. The relaxation process seemed to be in the activated regime, which was regarded as a tunneling from the thermally populated vibrational levels of the HS phase.[3d–g] The minimum of the first derivative of the $\chi_M T$ versus T plot gave a T(TIESST) value of 61 K.

Following this study of the metastable HS_2 state that was generated by a freezing effect, Figure 4 shows the time dependence of the quenched HS fraction (γ_{HS}) at selected temperatures. The kinetics curves showed a clear deviation from single exponential, whilst the relaxation rate was slow during a first stage and then accelerated in a second stage. This behavior was modeled by using a sigmoidal law that

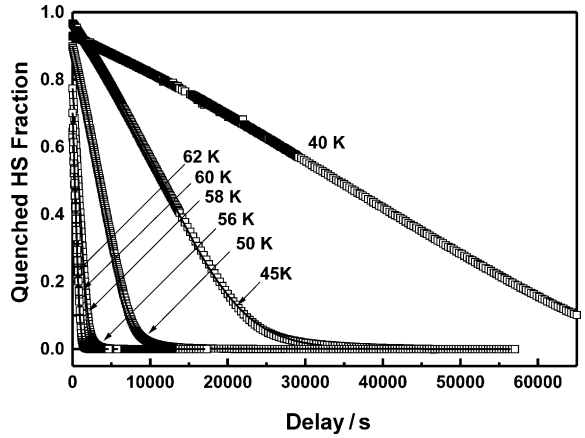

Figure 4. Time-dependence at various temperatures of the high-spin molar fraction that was generated by rapid freezing at 10 K. Each point represents the high-spin fraction from the magnetic response that was measured within the SQUID magnetometer for around 30 s. The relaxation curves are fitted according to sigmoidal behavior (Table 1).

was consistent with the predicted self-accelerated behavior for strongly cooperative systems.[3d–g,18] This cooperativity arises from the large difference in metal–ligand bond-lengths between the HS and LS states, thereby resulting in elastic interactions that are caused by the change in internal pressure inside the solids during the spin-transition processes. Thus, the height of the activation barrier to relaxation changes as a function of γ_{HS}, and the relaxation rate $k^*_{HL}(T, \gamma_{HS})$ depends exponentially on both γ_{HS} and T (Equations (1) and (2), where $\alpha(T)$ $(=E_a^*/k_BT)$ is the acceleration factor at a given temperature.

$$\frac{\partial \gamma HS}{\partial T} = k^*_{HL\gamma HS} \quad (1)$$

$$k^*_{HL}(T, \gamma_{HS}) = k_{HL}(T) \exp[\alpha(T)(1-\gamma_{HS})] \quad (2)$$

Based on this treatment, the calculated curves of the relaxation are shown as solid lines in Figure 4, and the fitted parameters are listed in Table 1. The apparent activation energy (E_a) and the apparent pre-exponential factor (k_∞) of the activated region were calculated from the straight line given by plotting $\ln k_{HL}(T)$ versus $1/T$.

Table 1. Thermodynamic parameters for thermal relaxation from metastable HS states that were generated at 10 K either by rapid freezing or by optical excitation.[a]

	k_∞ [s^{-1}]	E_a [cm^{-1}]	E_a* [cm^{-1}]
metastable HS_2 state	5×10^{-1}	300	60–110
metastable HS_3 state	1.8×10^{1}	350	60–80

[a] k_∞ and E_a are the pre-exponential factor and the activation energy of the activated region, respectively; E_a* is the additional activation energy that results from cooperativity.

Photoinduced metastable HS state, HS_3: The photomagnetic properties were studied by using a SQUID magnetometer that was connected to a CW optical source. A dramatic increase of the magnetic signal under light irradiation was observed at 10 K. Figure 5 shows the T(LIESST) curve. In this procedure, the irradiation was maintained until the signal was saturated, then the light was switched off, and the temperature was raised by 0.3 K min^{-1}. The minimum of the $d\chi_M T/dT$ versus T curve defined the limiting temperature, T(LIESST), above which the light-induced magnetic high-spin information was erased in a SQUID cavity.[6–9] The shape of the T(LIESST) curve was similar to that of the T(TIESST) curve (Figure 3): First, the $\chi_M T$ product increased upon warming from 10 K, owing to the zero-field splitting of the high-spin iron(II) ion, and reached a plateau at about 30 K. Comparison of the $\chi_M T$ value at the maximum of the T(LIESST) curve with the magnetic response that was recorded at room temperature indicated that, under bulk conditions, quantitative photoconversion occurred. The minimum of the $d\chi_M T/dT$ versus T curve was used to determine the limiting T(LIESST) temperature (61 K).

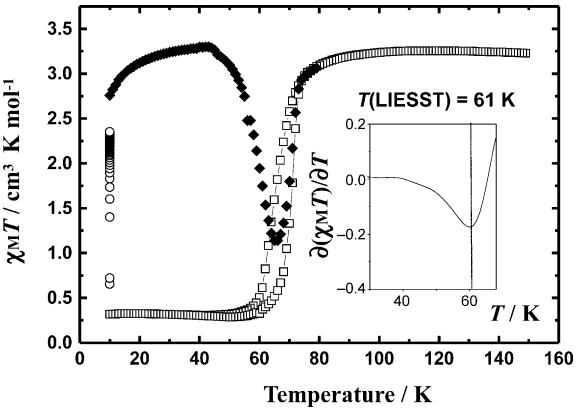

Figure 5. Temperature-dependence of the $\chi_M T$ value of the metastable HS state that was generated at 10 K by the LIESST effect. (□) Data recorded in the cooling and warming modes without irradiation; (○) data recorded with irradiation at 10 K; (◆) T(LIESST) values, data recorded in the warming mode with the laser turned off after irradiation for 1 h. Insets show the derivate of the $d\chi_M T/dT$ curves, whose minimum corresponds to the T(LIESST) temperature.

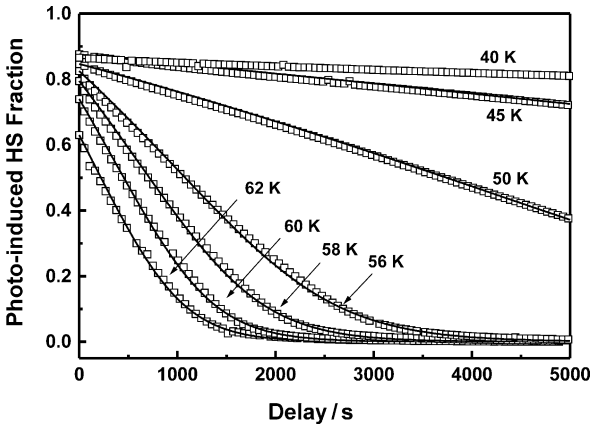

Figure 6. Time-dependence at various temperatures of the high-spin molar fraction that was generated by rapid freezing at 10 K. Each point represents the high-spin fraction from the magnetic response that was measured within the SQUID magnetometer for around 30 s. The relaxation curves are fitted according to sigmoidal behavior (Table 1).

Figure 6 shows the kinetic data that were recorded by using the SQUID magnetometer over the 40–60 K temperature range, in which the $HS_3 \rightarrow$LS state relaxation was thermally activated. The relaxation curves strongly deviated from single exponential and sigmoidal behavior was used. The calculated curves are shown as solid lines in Figure 6, and the fitted parameters are listed in Table 1. The photomagnetic properties of this complex appeared to be very close to the metastable HS_2 state that was generated by freezing. The only difference was in the stability of the two metastable states. Interestingly, the metastable HS_3 state that was generated by optical excitation was slightly more-stable than the metastable HS_2 state. This result was particularly emphasized by comparing the kinetic data at 40 K (cf. Figure 3 (HS_2) and Figure 6 (HS_3)). Over more than 12 h,

the relaxation of the metastable HS_3 state at 40 K represented only few percent, whilst for HS_2, almost 90% relaxation was observed. This difference was also manifested by carefully considering the shapes of the *T*(TIESST) and *T*-(LIESST) curves. In the latter case, the HS fraction was still relatively high when the warming branch of the thermal spin-transition was reached.

In 1998, it was reported that, under permanent irradiation, phase I of the $[Fe(PM\text{-}BiA)_2(NCS)_2]$ complex (PM-BiA = N-2′-pyridylmethylene-4-aminobiphenyl) displayed a new kind of thermal hysteresis in the vicinity of the *T*-(LIESST) temperature.[6a] This phenomenon was termed light-induced thermal hysteresis (LITH).[6a] More recently, Varret and co-workers reported a similar effect for the $[Fe_xCo_{1-x}(btr)_2(NCS)_2]\cdot H_2O$ system (btr = 4,4′-bis-1,2,4-triazole) and a nonlinear macroscopic master equation was proposed that was based on the competition between the constant photoexcitation and the self-accelerated thermal-relaxation process.[19] Figure 7 shows the LITH loop for *cis*-[Fe(picen)$(NCS)_2$]. Under permanent irradiation, the temperature was slowly cooled to 10 K at a rate of 0.1 K min^{-1} and then warmed to 100 K at a rate of 0.3 K min^{-1}. On first view, the shape of the LITH slope was relatively unusual. The HS fraction remained almost close to unity and the occurrence of the thermal spin-transition was almost absent. In fact, this latter property was masked by the population of the photoinduced HS state, owing to the close vicinity between the thermal spin-transition and the metastability region, which induced a very slow spin-equilibration. Thus, this optical stimulus was enough to almost maintain the HS state over the whole temperature range.

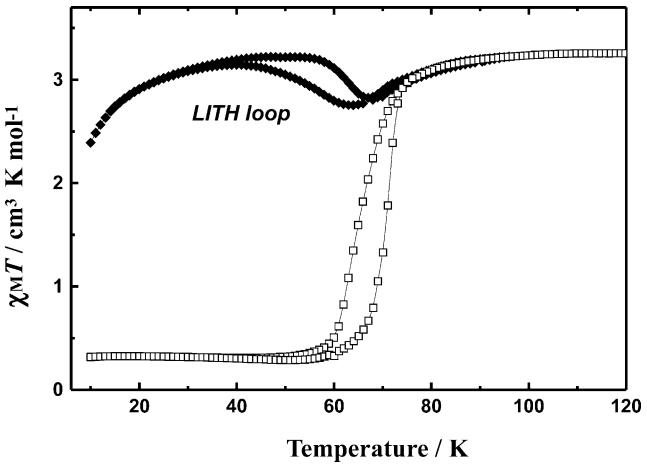

Figure 7. Temperature-dependence of the $\chi_M T$ value of the metastable HS state that was generated under continuous light irradiation in the cooling and warming modes (◆) and data recorded in the cooling and warming modes without irradiation (□).

Raman spectroscopy: Next, we attempted to directly observe the thermal- and light-induced spin-transitions by variable-temperature laser Raman spectroscopy. As previously indicated,[15] the Raman spectrum of *cis*-[Fe(picen)$(NCS)_2$] was characterized by two bands at around 2070 and 2100 cm^{-1} that were due to the C–N stretch of the NCS ligand (Figure 8). The lower- and higher-frequency bands corresponded to the high- and low-spin states, respectively. Nevertheless, the intensities of such Raman bands only slightly varied with temperature. The high-spin fractions were approximated as $n_{HS} = I_{HS}/(I_{HS}+I_{LS})$, where I_{HS} (of the high-spin species at around 2070 cm^{-1}) and I_{LS} (the low-spin species at around 2100 cm^{-1}) are Raman-integrated band-intensities at the observed temperatures. Plots of the high-spin fraction from the Raman-band intensities versus *T* did not behave in a similar manner to those obtained from the magnetic susceptibility ($\chi_M T$; Figure 2 and Figure 3). In contrast to the deep drop to 100% of the low-spin fraction between the transition temperatures, the picen complex only exhibited a shallow dip below $T_{1/2}$ (Figure 9), which reflected the slow relaxation from high- to low-spin and confirmed the shape of the LITH loop (Figure 7). Interestingly, the LIESST of the picen complex, which was reported to be about 40% by Mössbauer spectroscopy using broad-band (350–650 nm) excitation with a Xe arc lamp at 10 K,[14] was found to be almost quantitative by photomagnetic study and Raman spectroscopy, thus illustrating the importance of light penetration in such deep-colored materials for discussing the occurrence of the photoinduced metastable HS state.

X-ray diffraction: Variable-temperature single-crystal X-ray diffraction experiments were performed to determine the structure–property relationships and to investigate the thermal-spin-crossover mechanism. In addition, the photomagnetic behavior was explored by single-crystal X-ray diffraction at very low temperatures coupled with light irradiation of the sample. First, the crystal structure was solved in the high spin at a chosen temperature (120 K) that was close enough to the transition to minimize the thermal effects in front of the spin-crossover effects on the structural properties when subsequently comparing the HS and LS crystal structures. Then, the crystal structure was solved at 30 K, at which the sample was supposed to be made of a mixture of HS and LS spin states, depending on the cooling rate. For this reason, four structure-determinations were performed at 30 K, which corresponded to different cooling rates: true flash freezing[10a] was performed first and denoted as the "flash" crystal structure, then from 120 to 30 K speed cooling of 6, 0.5, and 0.05 K min^{-1} were used to give the "fast", "medium", and "slow" crystal structures, respectively. The light-irradiation experiment was performed starting from the slow conditions, thereby giving the "slow*" data (Table 2).

The crystal packing consisted of $[Fe(picen)(NCS)_2]$ sheets that were parallel to the *ac* plane (Figure 10). Intermolecular interactions built the cohesion of the crystal packing through π stacking and hydrogen bonding within the sheets and hydrogen-like bonding involving sulfur atoms between complexes of neighboring sheets. This overall description was similar in all of these above phases and was not affected

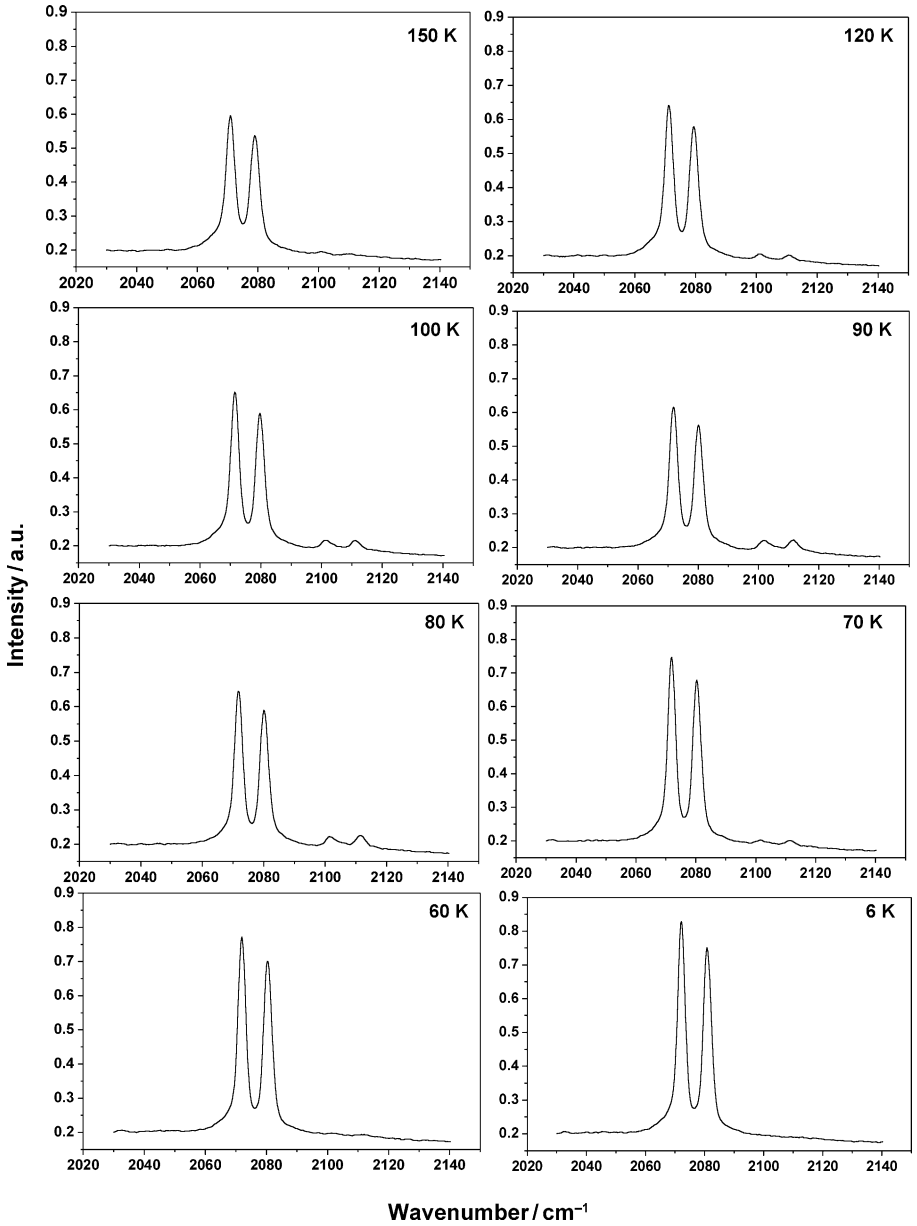

Figure 8. Temperature-dependence of the Raman spectra (excitation: 632.8 nm).

by the spin-conversion. However, the spin-conversion modified the unit cell parameters (Table 2); comparison of the HS and 30 K unit cells showed a significant decrease in the *a* and *c* parameters whilst *b* remained almost constant. This result indicated that the most-significant modifications in the crystal packing were due to the effect of spin-crossover on the intrasheet features. The unit-cell-volume modifications, which were also represented by the macroscopic-volume modification of the single crystal owing to spin-crossover,[20] was 3.7% between the HS 120 K and the LS slow unit cells, the latter being closer to a pure LS state. This volume decrease was perfectly in line with the typical values for mononuclear materials.

The spin-conversion obviously affected the intramolecular structural features and, in particular, the iron coordination-sphere geometry. It is well-established that spin-crossover corresponds to important changes in the Fe–N bond lengths and a modification of the metal coordination sphere.[20] For instance, going from HS to LS for the FeN_6 coordination spheres caused the Fe–N distance to shorten by about 0.2 Å and the iron environment to go from a strongly distorted octahedron (almost a trigonal prism) to a slightly distorted octahedron, with a corresponding decrease of 25% in volume during the transition. Table 2 lists the Fe–N bond lengths for $[Fe(picen)(NCS)_2]$ in all of the phases defined above. Because the asymmetric unit of $[Fe(picen)(NCS)_2]$ consisted of one complex, whatever the phase, there was only one crystallographically independent iron site in both the HS and LS states. As a consequence, the Fe–N bond lengths reflected an average of the HS and LS bond-lengths, with a relative weight that corresponded to the percentage of both species. Thus, from the Fe–N bond lengths, given pure HS and pure LS values, it was possible to estimate the percentage of spin-conversion (Table 3). The data at 120 K clearly showed a pure HS state whilst, as expected, other phases revealed a mixture of the HS and LS states at 30 K. The percentage of spin-conversion strongly correlated to the speed of cooling and warming between the flash, fast, medium, and slow modes: the slower the rate of cooling, the larger the conversion. Interestingly, in the Fast experiment, there was a small amount of HS-to-LS conversion, which meant that the spin-conversion could not be entirely quenched in a single crystal. The spin-conversion rate increased as the speed of cooling decreased and reached about 25% in the slow mode, which was slightly higher than expected from the magnetic measurements. To sum-up, this X-ray-diffraction cooling-rate study confirmed that the iron HS percentage decreased continuously when the rate of cooling slowed and that a direct correlation between the Fe–N bond length and the rate of spin-conversion was achievable.

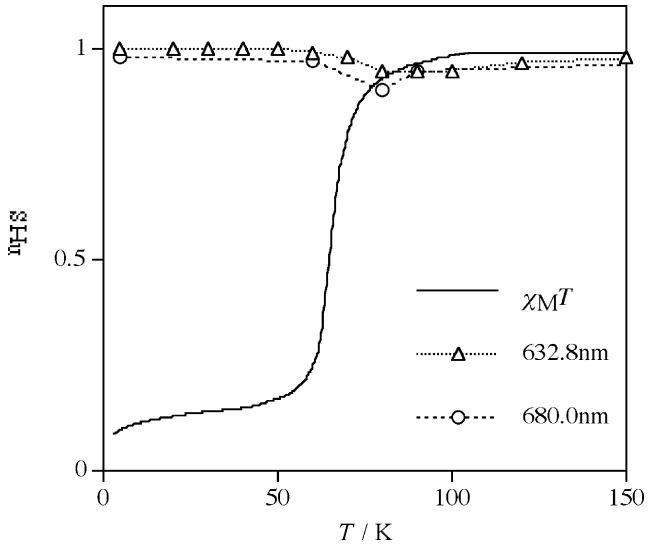

Figure 9. Temperature-dependence of the high-spin fraction (n_{HS}) that was obtained from the $\chi_M T$ and Raman spectra with excitation at 632.2 and 680 nm.

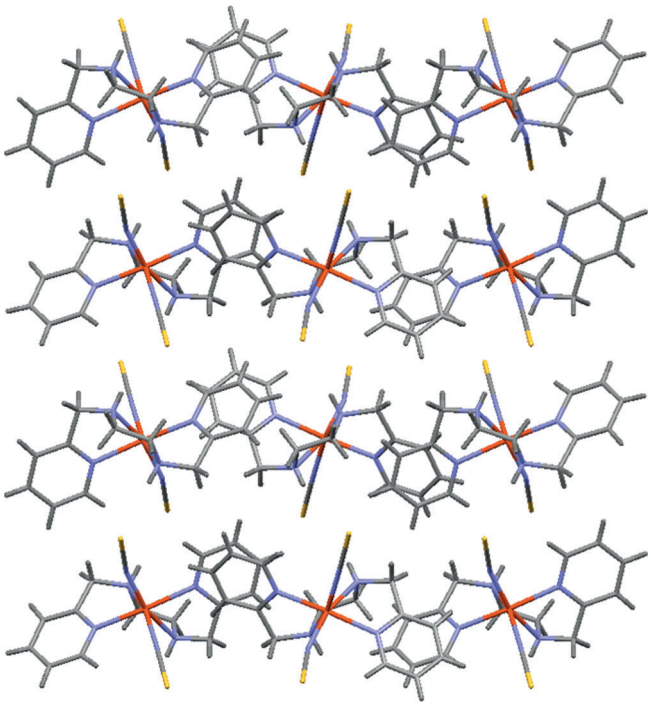

Figure 10. View along the *a* axis of the crystal packing of [Fe(picen)-(NCS)$_2$] at 120 K. The overall description was the same at lower temperatures.

In addition, this study revealed the mechanism of the spin phenomenon itself inside this compound. Indeed, because there was only one crystallographically independent iron site in the HS/LS phases, the LS sites must have been randomly distributed throughout the crystal structure: there was no ordering of the low-spin-state distribution. To this end, the atomic displacements parameters (ADPs) could provide important information about the system, and as such were worth examining. Their size and shape were dependent on several factors, two of the most-important being temperature and disorder.[21] From a crystallographic point of view, a random distribution of the structurally different HS and LS sites throughout the lattice manifested itself as a single crystallographically independent site with a large variation in the Fe–N bond lengths and angles at the iron center. This disorder in the spin states resulted in enlarged ADPs for the whole structure. The ADPs might have been expected to be largest when the ratio of the HS/LS sites was approximately equal. As mentioned previously, the structural features that underwent the most-pronounced change during spin-crossover were those that were directly associated with the FeN_6 coordination sphere; hence, it was the size of the ADPs of the nitrogen atoms that would yield the most information regarding the HS/LS ratio for structures that were collected at the same temperature. Figure 11 shows ADPs for all of the determined structures, along with average U_{iso} values for the N atoms in each structure.

Examination of the structures after flash, fast, medium, and slow cooling modes revealed larger ADPs than would normally be expected at 30 K, thereby reflecting the observed random distribution of spin states throughout the crystal under these conditions. The structure that was acquired after irradiation (slow*) showed significantly smaller ADPs than any of the other structures that were acquired at 30 K, which was consistent with a full photo-induced conversion into one single (HS) state. The ADPs for this structure were also much smaller than those in the only other fully HS structure, which was collected at 120 K, and were a direct result of the dif-

Table 2. Selected X-ray diffraction data for [Fe(picen)(NCS)$_2$] and the experimental parameters for all of the phases.

	HS	Flash	Fast	Medium	Slow	Slow*
T [K]	120	30	30	30	30	30
cooling rate [K min^{-1}]		instant	6	0.5	0.05	0.05
space group			$P2_1/n$			
a [Å]	9.237(1)	9.189(4)	9.154(2)	9.146(2)	9.107(2)	9.167(2)
b [Å]	13.761(1)	13.712(4)	13.696(2)	13.723(2)	13.742(2)	13.691(3)
c [Å]	14.653(2)	14.521(5)	14.461(2)	14.379(1)	14.318(1)	14.559(3)
β [°]	92.264(2)	92.399(5)	92.279(2)	91.972(2)	91.949(2)	92.621(3)
V [Å^3]	1861.1(5)	1828.0(9)	1811.6(6)	1803.4(6)	1790.9(6)	1825.4(7)
ρ_{calcd} [g cm^{-3}]	1.479	1.505	1.519	1.526	1.537	1.508
unique reflns (R_{int})	3269 (0.0414)	3731 (0.0558)	4105 (0.0513)	4071 (0.0428)	3716 (0.0484)	3228 (0.08)
R (all data)	0.039 (0.061)	0.037 (0.051)	0.0351 (0.0506)	0.039 (0.049)	0.038 (0.057)	0.044 (0.077)
wR_2 (all data)	0.0959 (0.0996)	0.0888 (0.0944)	0.0901 (0.0963)	0.0802 (0.0853)	0.0867 (0.0947)	0.086 (0.096)

Table 3. Fe–N bond lengths [Å], average Fe–N bond length (d [Å]), and the percentage (%) of the spin-state species at the iron site for all phases.[a]

	HS	Flash	Fast	Medium	Slow	Slow*
T [K]	120	30	30	30	30	30
Fe1–N1	2.199	2.164	2.121	2.081	2.026	2.188
Fe1–N2	2.214	2.195	2.154	2.119	2.027	2.212
Fe1–N3	2.236	2.213	2.145	2.106	2.114	2.231
Fe1–N4	2.206	2.171	2.117	2.079	2.036	2.186
Fe1–N5	2.087	2.073	2.035	2.010	1.961	2.115
Fe1–N6	2.108	2.095	2.051	2.031	2.026	2.099
d	2.1750	2.1518	2.1038	2.0708	2.0316	2.172
n_{HS} (%)	100	88	64	48	28	99
n_{LS} (%)	0	12	36	52	72	1

[a] The percentage of spin-state species was calculated from d by using the formula $n_{HS}=(d-d_{LS})/(d_{HS}-d_{LS})$ with $d_{HS}=2.175$ and $d_{LS}=1.975$, which are the d values for pure HS and LS states, respectively; d_{HS} was known from the high-temperature structure, d_{LS} could not be strictly known for this compound but it was taken as an average of typical values in iron materials. Errors in n_{HS} and n_{LS} were estimated to be 5–10% for all data at 30 K.

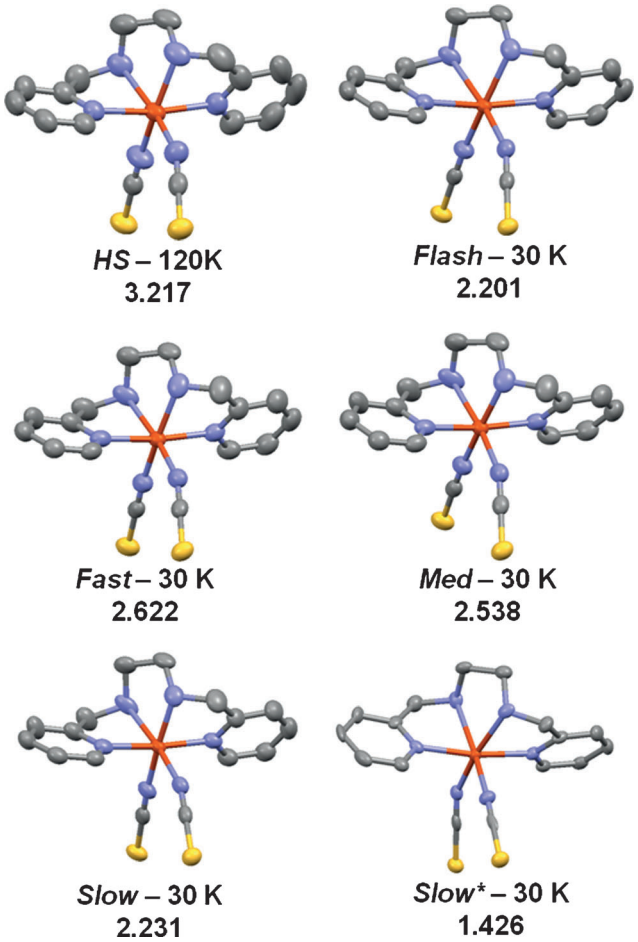

Figure 11. Molecular structure with atomic displacement parameters (ADPs) of [Fe(picen)(NCS)$_2$] and average U_{iso} values (10^{-2} Å^2) for the nitrogen atoms at 120 K and 30 K after various cooling and light-irradiation regimes. ADPs are drawn at 80% probability.

ference in temperature between these two measurements. To conclude, the random-spin-state-distribution mechanism was clearly revealed by the X-ray-diffraction study of [Fe(picen)(NCS)$_2$], and the relative proportion of HS and LS states was determined by using structural methods.

Elsewhere, the photoinduced HS crystal structure (slow*) appeared to be very close to the high-temperature HS structure. Such a similarity is typically the case when no structural phase-transition with a change of symmetry is associated to the spin-crossover. However, the unit-cell parameters showed some differences that were attributed to thermal effects on the crystal packing. It was possible, starting from the slow* phase at 30 K, to follow the relaxation to the LS state and then the thermal spin-crossover from the warming of the single crystal from 30 K to 90 K (Figure 12). The observed structural behavior was perfectly coherent with the magnetic properties, which showed the vicinity of the temperature area of the light-induced and thermal spin-crossover phenomena.

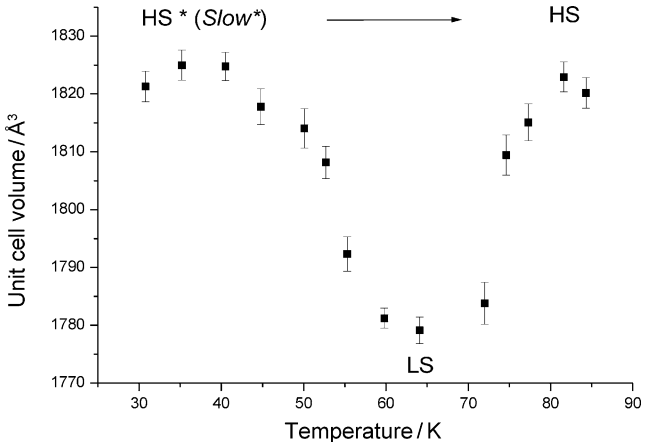

Figure 12. Temperature dependence of the unit cell volume from the 30 K photoinduced spin state unit cell (slow*) to the HS unit cell, which shows the HS* to LS relaxation and thermal spin-crossover.

Conclusion

Thermal spin-crossover of *cis*-[Fe(picen)(NCS)$_2$] (picen = *N*,*N*′-bis(2-pyridylmethyl)1,2-ethanediamine) occurred in the close vicinity of the metastable region of the HS state, that is, HS$_2$ and HS$_3$, which were either generated by freezing or by light stimulation. As a consequence, the spin-equilibration in this compound was extremely slow and the residual HS fraction at low temperatures strongly depended on the cooling speed. Only at cooling speeds slower than 0.1 K min^{-1} did an almost-complete abrupt thermal spin-transition occur at about 70 K, with only a residual HS fraction of about 0.09 at 40 K. Nevertheless, even at such a slow cooling rate, the shape of the thermal hysteresis remained unsymmetrical. By recording long kinetic relaxations at various temperatures in the range 60–70 K, we were able to extrapolate the shape of the quasi-static thermal hysteresis loop, which appeared to be symmetric in this case.

The high potential of this compound to exhibit metastability at low temperatures was used for comparing the characteristics of HS states that were generated by freezing (HS_2) and by light irradiation (HS_3). The kinetic parameters that governed the relaxation process indicated that the two metastable HS states were closely related, although a higher stability for the photoinduced HS state was observed. Very few reports have performed such a systematic comparison for a spin-crossover material.

The close vicinity of the thermal spin-transition and the relatively slow relaxation process also allowed us to report an unusual shape of the LITH loop, in which the HS fraction always remained very high. This effect was also confirmed by Raman spectroscopy, which found that, whatever the investigated temperature, the recorded spectrum was almost always typical of the HS state. In this compound, the spin-equilibration was so slow that any optical stimulus was enough for maintaining the HS state.

Single-crystal X-ray diffraction allowed us to elucidate the phase diagram as a function of speed-cooling and light irradiation. The phase diagram showed a direct relationship between the geometry of the metal coordination sphere and the degree of spin-conversion. The determination of X-ray structures in various degrees of spin state at 30 K, from 100% HS to about 30% HS, revealed a spin-conversion mechanism that consisted of a random distribution of LS sites throughout the lattice. Without doubt, this mechanism endowed some flexibility to this material on the macroscopic level, thereby explaining the avoidance of cracking of the crystalline sample when it was driven by temperature effects in a mixture of HS and LS spin states. In addition, this crystallography study also confirmed the vicinity of the light-induced and thermal spin-transitions.

In summary, this work emphasizes that, when the thermal spin-transition occurs in the close vicinity of the metastability regime, some synergetic effects may happen; that is, the kinetics of the metastable HS state (that is either generated by light irradiation or by freezing) overlap with the thermal transition and, as a consequence, the SCO phenomenon may appear "hidden".[22–25] Let us mention three recent contributions that highlight this effect: The first concerned the $[FeL_2](BF_4)_2{\cdot}xH_2O$ complex (L = 2,6-bis{3-methylpyrazol-1-yl}pyridine; $x = 0$–1/3), which exhibited a thermal spin-transition in two steps that were centered at 147 and 105 K, very close to the T(LIESST) value of 87 K.[22] A magnetic-susceptibility experiment revealed only 54% spin-conversion, but a special thermal treatment between the T(LIESST) value and the $T_{1/2}$ temperatures, that is, at 100 K for 2 h, resulted in a slow decrease of the $\chi_M T$ product to zero, thus showing that the remainder of the spin-crossover can proceed but is kinetically slow.[22] The second report involved metal-dilution in the $[Fe_xMn_{1-x}(bpp)_2](NCSe)_2$ series.[23] We have demonstrated that, in the case of high metal dilution with $x < 0.2$, $T_{1/2}$ can reach T(LIESST). In this peculiar situation, where the thermodynamically stable HS region reached the metastable HS region, the complex remained HS over the whole temperature range. The third example involved the systematic determination of the $T_{1/2}$ and T(LIESST) temperatures for a series of SCO dinuclear complexes.[24] The peculiar case of the $[\{Fe(NCBH_3)(3,5\text{-diMepy})\}_3(bpypz)_2]$ dinuclear complex, which remained HS whatever the temperature, was attributed to the physical impossibility that the T(LIESST) value became higher than $T_{1/2}$. To check this hypothesis of the close vicinity of the thermal-spin-crossover phenomenon, we applied hydrostatic pressure, which is well-known for stabilizing the LS state of the smaller volume. At 9.9 kbar, the thermal spin-transition was found, and around 70% of the complex switched into the LS electronic configuration.[24] All of these results confirmed that the relationship between the T(LIESST) and $T_{1/2}$ values represents a real guideline that allows us to both predict the stability of the photoinduced HS state and to understand the synergetic effects that occur when the two regions are collapsing. The challenge now is to shift the limiting temperature to above room temperature, but for that we should scrupulously study various SCO materials to identify the key factor(s) that are acting on the stability of the metastable HS state. In less than 10 years, the T(LIESST) temperature of SCO materials has been improved from 30 K to almost 130 K,[26] and even 150 K in Prussian blue analogues.[27] The record today is held by a molecular cluster with a value of about 180 K.[28] The rigidity and the distortion of the inner coordination sphere appear to be the crucial factors.

Experimental Section

***N,N′*-bis(2-pyridylmethyl)ethylenediamine (picen)**: Zinc powder (6.7 g) was stirred in a solution of ethylenediamine (1.0 g, 1.67×10^{-2} mol), EtOH (40 mL), and glacial acetic acid (7 mL) at 60–70 °C and a solution of 2-pyridinecarboxaldehyde (3.6 g, 3.33×10^{-2} mol) in EtOH (20 mL) was gradually added over 2 h. Zinc powder and glacial acetic acid were added at intervals until a further 23.3 g of each had been added and the reaction was stirred for a further 24 h. The mixture was allowed to stand at room temperature overnight and was then filtered. The filtrate was evaporated to afford a syrupy residue before sodium hydroxide was added. A brown oil separated and was collected, dried overnight in diethyl ether with anhydrous magnesium sulfate, and concentrated in vacuo to obtain a yellowish oil. The product was used without further purification.

$[Fe(picen)(NCS)_2]$: Because of the air-sensitivity of Fe^{II} species, the synthesis of the complex was carried out under a nitrogen atmosphere using standard Schlenk techniques.

$[Fe(SCN)_2]$ was prepared in situ by reacting an iron salt with a thiocyanate anion. A solution of KNCS (2 mmol) in MeOH (50 mL) was added to a mixture of solutions of $FeCl_2{\cdot}4H_2O$ (1 mmol) in MeOH and a small amount of ascorbic acid as a reducing agent in MeOH (50 mL). The solution was stirred for 20 min and the resulting white precipitate (KCl) filtered off by using a cannula filter. The colorless solution of $[Fe(SCN)_2]$ was mixed with a solution of picen (1 mmol) in MeOH (100 mL), and the color of the solution changed to yellow. The resulting mixture was left undisturbed for 1 day at room temperature. Yellow crystals were formed and were collected by suction filtration and dried under vacuum (75% yield).

Magnetic and photomagnetic studies: The measurements were performed on a Spectrum Physics mixed-gas Ar/Kr laser ($\lambda = 532$ nm) that was coupled via an optical fiber to the cavity of a MPMS-55 Quantum Design SQUID magnetometer and the power at the sample surface was adjusted to 5 mW cm^{-2}. The samples consisted of a thin layer of compound, the

weight of which was obtained by comparison of the thermal spin-crossover curve with that of a more-accurately weighed sample of the same compound. Our previously reported standardized method for determining LIESST properties was followed.[6–9] After cooling slowly to 10 K, the sample in the LS state was irradiated and a change in magnetism occurred. When the saturation point had been reached, the light was switched off, the temperature was increased at a rate of 0.3 K min^{-1}, and the magnetization was measured every 1 K. T(LIESST) was determined from the minimum of the $\delta\chi_M T/\delta T$ versus T curve for the relaxation process.

Raman spectroscopy: Raman spectra were recorded for powdered samples by using a Raman-excitation HeNe, Ar, or Dye CW unfocused laser beam (f1 mm; about 3 mW) with 32 times accumulation every 20 s by a Jasco NR-1800 Raman spectrophotometer. Variable-temperature Raman spectroscopy was performed by using an Oxford CF1204 cryostat.

X-ray diffraction: Single-crystal structure-determination was carried out from X-ray data that were collected at 120 K and 30 K by using graphite-monochromated $Mo_{K\alpha}$ radiation ($\lambda = 0.71073$ Å) on a Bruker SMART-CCD 1 K diffractometer. A series of narrow ω-scans (0.3°) was performed at several ϕ-settings in such a way as to cover a sphere of data to a maximum resolution of 0.70 Å. Cell parameters were determined and refined by using SMART software,[29] and raw frame data were integrated with the SAINT program.[30] The structures were solved by direct methods using SHELXS, and refined by full-matrix least-squares on F^2 using SHELXL-97[31] and the graphical user interface Olex2.[32] The temperature was controlled by a Cryostream N_2 open-flow cooling device[33] (for the 120 K dataset) and an Oxford Cryosystems Helix[34] (an open-flow He cooling device) for the 30 K datasets. The same crystal was used for the high-spin, flash, fast, medium, and slow diffraction experiments, with the slow* experiment being performed on a different crystal of similar size and quality. The crystal was mounted in an inert oil at room temperature and was cooled at 2 K min^{-1} to 120 K where the data were either collected (HS experiment) or further cooled at 6, 0.5, or 0.05 K min^{-1} to 30 K (fast, med, and slow experiments, respectively). The flash experiment was performed by flash freezing the crystal from room temperature to 30 K.

Acknowledgements

The authors would like to thank the GIS-Advanced Materials in Aquitaine (AMA), the ANR Agency (ULTiMATE and SCOOP), the CEFIPRA, and the Aquitaine Region for supporting the development of the ICPA platform at the International Center of Photomagnetism in Aquitaine. We also gratefully thank the PHC ALLIANCE program for funding the exchange between the Université Bordeaux and the University of Durham.

[1] a) G. E. Moore, *Electronics* **1965**, *38*, 114; b) G. E. Moore in *Digest of the 1975 International Electron Devices Meeting*, IEEE, New York, **1975**, 1113; c) R. P. Feynman, *Eng. Sci.* **1960**, *23*, 22; d) F. M. Raymo, *Adv. Mater.* **2002**, *14*, 401.

[2] a) For general reviews, see: P. Gütlich, H. A. Goodwin, *Spin Crossover in Transition Metal Compounds I-III, Top. Curr. Chem.*, Springer, Vienna, **2004**, *Vols. 233–235*; b) P. Gütlich, A. Hauser, H. Spiering, *Angew. Chem.* **1994**, *106*, 2109; *Angew. Chem. Int. Ed. Engl.* **1994**, *33*, 2024; c) P. Gütlich, Y. Garcia, T. Woike, *Coord. Chem. Rev.* **2001**, *219–221*, 839.

[3] a) J. J. McGravey, I. Lawthers, *J. Chem. Soc. Chem. Commun.* **1982**, 906; b) S. Decurtins, P. Gütlich, C. P. Köhler, H. Spiering, A. Hauser, *Chem. Phys. Lett.* **1984**, *105*, 1; c) A. Hauser, P. Gütlich, H. Spiering, *Inorg. Chem.* **1986**, *25*, 4245–4248; d) A. Hauser, *Coord. Chem. Rev.* **1991**, *111*, 275–290; e) A. Hauser, *Comments Inorg. Chem.* **1995**, *17*, 17–40; f) A. Hauser, *Top. Curr. Chem.* **2004**, *234*, 155; g) A. Hauser, C. Enaschescu, M. L. Daku, A. Vargas, N. Amstutz, *Coord. Chem. Rev.* **2006**, *250*, 1642.

[4] a) E. Freysz, S. Montant, S. Létard, J.-F. Létard, *Chem. Phys. Lett.* **2004**, *394*, 318; b) S. Bonhommeau, G. Molnár, A. Galet, A. Zwick, J. A. Real, J. J. McGarvey, *Angew. Chem.* **2005**, *117*, 4137; *Angew. Chem. Int. Ed.* **2005**, *44*, 4069.

[5] a) O Kahn, C Jay-Martinez, *Science* **1998**, *279*, 44; b) J.-F. Létard, P. Guionneau, L. Goux-Capes, *Top. Curr. Chem.* **2004**, *235*, 221.

[6] a) J.-F. Létard, P. Guionneau, L. Rabardel, J. A. K. Howard, A. E. Goeta, D. Chasseau, O. Kahn, *Inorg. Chem.* **1998**, *37*, 4432; b) J.-F. Létard, L. Capes, G. Chastanet, N. Moliner, S. Létard, J. A. Real, O. Kahn, *Chem. Phys. Lett.* **1999**, *313*, 115; c) S. Marcén, L. Lecren, L. Capes, H. A. Goodwin, J.-F. Létard, *Chem. Phys. Lett.* **2002**, *358*, 87.

[7] a) V. A. Money, J. S. Costa, S. Marcén, G. Chastanet, J. Elhaik, M. A. Halcrow, J. A. K. Howard, J.-F. Létard, *Chem. Phys. Lett.* **2004**, *391*, 273; b) C. Carbonera, J. S. Costa, V. A. Money, J. Elhaik, J. A. K. Howard, M. A. Halcrow, J.-F. Létard, *Dalton Trans.* **2006**, 3058.

[8] a) J.-F. Létard, G. Chastanet, O. Nguyen, S. Marcen, M. Marchivie, P. Guionneau, D. Chasseau, P. Gütlich, *Monatsh. Chem.* **2003**, *134*, 165; b) *Molecular Magnets Recent Highlights* (Eds.: W. Linert, M. Verdaguer), Springer, NewYork, **2003**, p. 49; c) J.-F. Létard, J. S. Costa, S. Marcen, C. Carbonera, C. Desplanches, A. Kobayashi, N. Daro, P. Guionneau, *J. Phys. Conf. Ser.* **2005**, *21*, 23.

[9] a) J.-F. Létard, P. Guionneau, O. Nguyen, J. S. Costa, S. Marcén, G. Chastanet, M. Marchivie, L. Capes, *Chem. Eur. J.* **2005**, *11*, 4582; b) J.-F. Létard, *J. Mater. Chem.* **2006**, *16*, 2550.

[10] a) M. Marchivie, P. Guionneau, J. F. Létard, D. Chasseau, J. A. K. Howard, *J. Phys. Chem. Solids* **2004**, *65*, 17–23; b) P. Guionneau, M. Marchivie, G. Bravic, J.-F. Létard, D. Chasseau, *Top. Curr. Chem.* **2004**, *234*, 97.

[11] a) J. S. Costa, C. Balde, C. Carbonera, D. Denux, A. Wattiaux, C. Desplanches, J. P. Ader, P. Gütlich, J.-F. Létard, *Inorg. Chem.* **2007**, *46*, 4114; b) P. Guionneau, J. S. Costa, J.-F. Létard, *Acta. Crystallogr. Sect. C* **2004**, *60*, m587m589; c) J. S. Costa, P. Guionneau, J.-F. Létard, *J. Phys. Conf. Ser.* **2005**, *21*, 67–72; d) S. Bonhommeau, T. Guillon, L. M. L. Daku, P. Demont, J. S. Costa, J.-F. Létard, G. Molnar, A. Bousseksou, *Angew. Chem.* **2006**, *118*, 1655–1659; *Angew. Chem. Int. Ed.* **2006**, *45*, 1625–1629.

[12] S. Bonhommeau, N. Bréfuel, V. K. Pálfi, G. Molnár, A. Zwick, L. Salmon, J.-P. Tuchagues, J. S. Costa, J.-F. Létard, H. Paulsen, A. Bousseksou, *Phys. Chem. Chem. Phys.* **2005**, *7*, 2909–2914.

[13] a) H. Toftlund, E. Pedersen, S. Yde-Andersen, *Acta Chem. Scand. A* **1984**, *38*, 693; b) H. Toftlund, *Coord. Chem. Rev.* **1989**, *94*, 67–108.

[14] T. Buchen, H. Toflund, P. Gutlich, *Chem. Eur. J.* **1996**, *2*, 1129–1133.

[15] N. Suemura, M. Ohama, S. Kaizaki, *Chem. Commun.* **2001**, 1538–1539.

[16] O. Kahn, *Molecular Magnetism*, VCH, New York, **1993**.

[17] E. Bukhs, G. Navon, M. Bixon, J. Jortner, *J. Am. Chem. Soc.* **1980**, *102*, 2918.

[18] a) A. Hauser, *Chem. Phys. Lett.* **1992**, *192*, 65; b) A. Hauser, J. Jeftic, H. Romstedt, R. Hinek, H. Spiering, *Coord. Chem. Rev.* **1999**, *190–192*, 471.

[19] A. Desaix, O. Roubeau, J. Jeftic, J. G. Haasnoot, K. Boukheddaden, E. Codjovi, J. Linarès, M. Nogues, F. Varret, *Eur. Phys. J. B* **1998**, *6*, 183.

[20] J. F. Létard, M. Kollmansberger, C. Carbonera, M. Marchivie, P. Guionneau, *C. R. Chim.* **2008**, *11*, 1155–1165.

[21] C. C. Wilson, *Crystallogr. Rev.* **2009**, *15*, 3–58.

[22] V. A. Money, C. Carbonera, M. A. Halcrow, J. A. K. Howard, J.-F. Létard, *Chem. Eur. J.* **2007**, *13*, 5503.

[23] C. Baldé, C. Desplanches, P. Gütlich, E. Freysz, J.-F. Létard, *Inorg. Chim. Acta* **2008**, *361*, 3529.

[24] J.-F. Létard, C. Carbonera, J. A. Real, S. Kawata, S. Kaizaki, *Chem. Eur. J.* **2009**, *15*, 4146–4155.

[25] H. Tokoro, S. I. Ohkoshi, *Appl. Phys. Lett.* **2008**, *93*, 021906.

[26] S. Hayami, Z.-Z. Gu, Y. Einaga, Y. Kobayashi, Y. Ishikawa, Y. Yamada, A. Fujishima, O. Sato, *Inorg. Chem.* **2001**, *40*, 3240.

[27] a) N. Shimamoto, S.-S. Ohkoshi, O. Sato, K. Hashimoto, *Inorg. Chem.* **2002**, *41*, 678; b) R. Le Bris, C. Mathonière, J.-F. Létard, *Chem. Phys. Lett.* **2006**, *426*, 380.

[28] D. Li, R. Clérac, O. Roubeau, E. Harte, C. Mathonière, R. Le Bris, S. M. Holmes, *J. Am. Chem. Soc.* **2008**, *130*, 252.
[29] SMART-NT, Data Collection Software, Version 6.1, Bruker Analytical X-ray Instruments Inc., Madison, WI, USA, **2000**.
[30] SAINT-NT, Data Reduction Software, Version 6.1, Bruker Analytical X-ray Instruments Inc., Madison, WI, USA, **2000**.
[31] G. M. Sheldrick, *Acta Crystallogr. Sect. A* **2008**, *64*, 112–122.
[32] O. V. Dolomanov, L. J. Bourhis, R. J. Gildea, J. A. K. Howard, H. Puschmann, *J. Appl. Crystallogr.* **2009**, *42*, 339–341.
[33] J. Cosier, A. M. Glazer, *J. Appl. Crystallogr.* **1986**, *19*, 105.
[34] A. E. Goeta, L. K. Thompson, C. L. Sheppard, S. S. Tandon, C. W. Lehmann, J. Cosier, C. Webster, J. A. K. Howard, *Acta Crystallogr. Sect. C* **1999**, *55*, 1243.

Received: August 24, 2011
Revised: December 31, 2011
Published online: March 27, 2012

